AN ABSTRACT OF THE THESIS OF

Tao Lyu for the degree of Master of Science in Electrical and Computer Engineering presented on March 11, 2016.

Title: Threshold Selection Based on The SNR in Time of Arrival Localization System

Abstract approved: _____

Huaping Liu

Threshold-based time of arrival (TOA) estimation is a technique for high-precision indoor localization. Existing threshold selection methods, such as fixed threshold and normalized threshold methods, do not consider the signal-to-noise radio (SNR) value at the receiver. This is not desired for high-precision positioning. A proper threshold value depends on the statistics of the received signal. The dominating parameter that affects the statistics of the receiver is the SNR. In this thesis, we propose an adaptive threshold selection method which takes the SNR value at the receiver into consideration, resulting in an increased precision of the timing detection (first peak detection). The performance of the proposed method is evaluated in simulation. The simulation uses ultra wideband transmitted signal, and adopts the IEEE 802.15.3a channel model. Performance of the normalized threshold method and the proposed selection threshold method are compared.

Threshold Selection Based on The SNR in Time of Arrival Localization System

by

Tao Lyu

A THESIS

submitted to

Oregon State University

in partial fulfillment of
the requirements for the
degree of

Master of Science

Presented March 11, 2016
Commencement June 2016

Master of Science thesis of Tao Lyu presented on March 11, 2016.

APPROVED:

Major Professor, representing Electrical and Computer Engineering

---

Director of the School of Electrical Engineering and Computer Science

---

Dean of the Graduate School

I understand that my thesis will become part of the permanent collection of Oregon State University libraries. My signature below authorizes release of my thesis to any reader upon request.

Tao Lyu, Author

ACKNOWLEDGEMENTS

First of all, my deepest and most sincere appreciation to Dr. Huaping Liu as my major professor, his guidance and advice has been very important and helpful. Without his advising, I couldn't complete this thesis work. Also, I would like to express the same appreciation to all my committee members, Dr. Thinh Nguyen, Dr. Alan Wang and Dr. Williams H. Warnes, with their timely help I was able to set up the final oral exam.

I must also thank all the group members in Dr. Liu's group, Xuanyi Dong, Zhenqiang Su, Younghoon Whang, Deyan Chen, Guangxin Wang and others. They applied me with very helpful information and suggestion during my work and studies. The same to all my friends at OSU, Ziwei Ke, Jimmy Chen, Qiwei Wang, Cheng Li, Lawrence Eng, Jia Wan, Teng Ma, David Leu who gave me warmly helped and support in my life in Corvallis.

Also, the same appreciation goes to all people in Church of Corvallis, especially to Donald Orwick, Hsichao Chow, Jim Sedgwick and others. Their strong supports have given me great courage to overcome the troubles I met.

Last, the special appreciation for my parents, I couldn't survive in the US these years without their selfless dedication.

TABLE OF CONTENTS

TABLE OF CONTENTS (Continued)

LIST OF FIGURES

LIST OF FIGURES (Continued)

LIST OF TABLES

Chapter 1: Introduction

Location awareness has received a great deal of interest in many wireless systems such as cellular networks, wireless local area networks, and wireless sensor. Geometric localization methods include time of arrival (TOA), time difference of arrival (TDOA), received signal strength (RSS) and angle of arrival (AOA). TOA has drawn great interest among these methods since it has a high potential to achieve high-precision [1]. Threshold-based estimator, one of TOA estimators, is the most popular TOA estimator due to its simple implementation [2].

The estimation process of the threshold-based method includes three major parts: ranging, positioning, and tracking [1]. The ranging part is the first step for TOA estimation [1], so the accuracy of ranging directly affects the accuracy of TOA estimation.

Timing detection is the major part of the ranging process, and a proper threshold selection has significant effect on the precise of timing detection [3]. Threshold selection has been investigated extensively in the literature. However, some open issues remain unresolved. The threshold value should depend on the received signal-to-noise ratio (SNR). One of the main challenges is selecting a proper threshold according to the SNR at the receiver. Previous literature has applied the fixed threshold and the normalized adaptive threshold methods [4, 5]. None of these methods take into consideration of the SNR value at the receiver.

This thesis develops a threshold selection method that takes the received SNR value into consideration. Also, the process of theory development of this method, and the performance of this method will be introduced in this thesis.

The background knowledge of localization system is in Chapter 2, which includes the basic localization methods, the basic TOA approaches, the common threshold selection methods, and the channel model. Chapter 3 introduces the theory part of relating the threshold selection to the SNR value at the receiver side, including the motivation of this thesis, the theory developing process, and the theory of the proposed threshold selection method. In Chapter 4, the simulation setting, process and the simulation result are presented. It includes the error analysis of the proposed threshold selection method via simulation results. Also, comparison result between the proposed threshold selection method and the normalized adaptive threshold methods is presented at the end of this chapter. The last chapter conclude the work of this thesis, and discusses potential future development of the SNR related threshold-based method.

Chapter 2: Background Review

2.1 Basic Localization Method

Indoor location-based applications have received significant interests recently. Such services include location based advertisement, location based social networking, and E911 emergency services. Take the E911 emergency services for example, the user will be able to make emergency calls that allow local authorities to pinpoint the user's position in indoor scenarios.

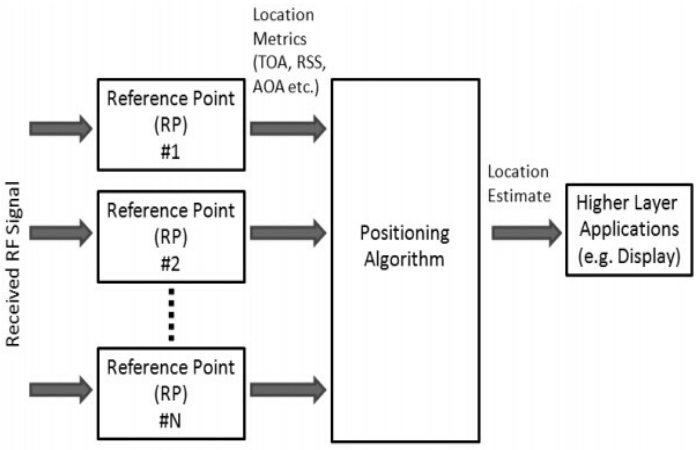

Figure 2.1: General architecture of localization systems.

In common cases, a localization system consists of moving terminals to be

tracked, anchors serving as reference points (RPs), and a central processing station that implements the positioning algorithm and keeps track of all the terminals. Figure 2.1 shows such a localization system. Different methods (i.e., TOA/TDOA, RSS, AOA) could be used for positioning.

Localization may be realized in two common ways [1]:

1. Geometric methods (trilateration, triangulation, hyperbolic methods)
2. Fingerprinting methods (signal mapping)

Geometric methods can locate devices based on the estimated signal properties. TOA/TDOA, RSS and AOA are examples of geometric measurement techniques.

2.1.1 Received signal strength

RSS ranging is based on the principle that the greater the distance between the fixed terminals (FTs) and the moving terminal (MTs), the weaker their relative received signals [6]. The ranging distance is measured based on the attenuation from FTs to MTs. Since the relationship between the distance and the attenuation depends on channel behavior, an accurate propagation model is required for reliable distance estimation.

A commonly used model to estimate the RSS is expressed as [6]

$$P(d) = P_0 - 10\gamma \log_{10} d + S \tag{2.1}$$

where $P(d)$ is the received power, related to the distance between the FT and the MT d, with unit dBm; P_0 is the received power (the unit is dBm) at the reference distance, which is a function of the signal wavelength, and the radio charactieristics [6]; γ is known as the path-loss exponent, and the value of γ is typically in the range of 2 to 6 [6]; $S(dB)$ is the large-scale fading variable (i.e., shadowing).

The main advantage is the simplicity of its implementation [7]. However, the practical propagation environments cause the attenuation of the signal to poorly correlate with distance, resulting in inaccurate distance estimates [7].

This technique is commonly used in low-cost systems such as wireless sensor networks (WSNs) because hardware requirements and costs can be more favorable compared to time-based techniques [6]. However, RSS based methods are easy to implement but in general inaccurate [8].

2.1.2 Angle of arrival

AOA forms a radial line from the reference node to the target node to be positioned [7]. For two-dimensional (2-D) positioning, AOA estimates the target position by finding out the intersection of two directional lines of bearing [6, 7, 9, 10], as illustrated in Figure 2.2.

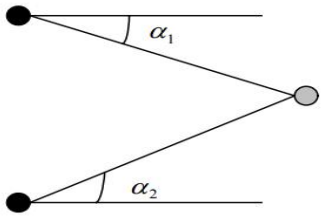

Figure 2.2: AOA measurement.

The two black dots in Figure 2.2 are the reference nodes (RNs), the gray point is the target node (TN), and α_1, α_2 are the AOAs. The two RNs measure the angles between themselves and the TN, α_1 and α_2.

Antenna arrays are commonly used to implement the AOA method. The main idea for this measurement is that the difference of the arrival times at different antenna elements contains the angle (phase) information for a known geometry [6, 7, 9, 10].

However, the AOA method requires a different hardware between the antenna elements to get the unique phase information for large bandwidth signal, which results in additional costs [6, 7, 10]. Additionally, AOA is highly sensitive to the multipath environment, and array precision [7].

2.1.3 Time of arrival

TOA technique is in general more complex than RSS and AOA methods, but they can potentially provide a much higher localization accuracy [11, 12].

When the direct path (DP) is detectable, the arrival time of the DP is the TOA.

When a DP is not available or undetectable, other components in a multipath environment may be used for ranging. The distance between the terminal and RP equals the TOA value time the speed of the light. This is written as:

$$d = c\tau \tag{2.2}$$

where τ is the time of arrival of the first peak or the direct path, c is the speed of light. The basic principle of TOA in 2-D can be shown in Figure 2.3.

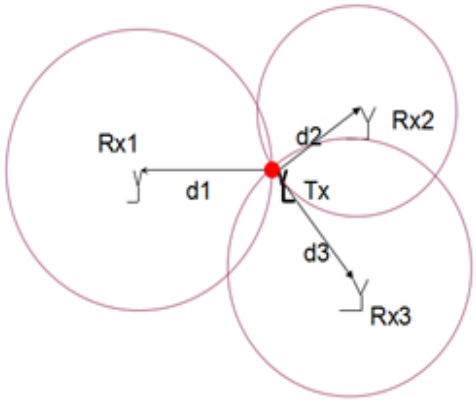

Figure 2.3: A 2-D TOA measurement.

In Figure 2.3, Rx_1 to Rx_3 are FTs, Tx is the MT, and d_1 to d_3 are measured distances between Tx and each of Rx. d_1 to d_3 can be evaluated by getting the estimated time. Circles could be drawn by knowing the value of d_1 to d_3, then the intersection of three circles is the position of MT.

TOA includes one-way TOA and two-way TOA. For one-way TOA: at a random time t_a, terminal A transmits to receiving terminal B a packet that contains

the time-pin t_a at which As packet was sent. Terminal B receives the packet at time t_b. Under ideal conditions, that is, when terminals' clocks are perfectly synchronized to a common time reference, it is clear that time difference t_f can be determined at terminal B as $t_f = t_b - t_a$, from which the distance can be estimated [6]. Synchronization error could significantly affect ranging accuracy [6].

For two-way TOA: the system estimates the signal round-trip time (RTT) t_{RT} without a common time reference. Terminal A transmits a packet to terminal B, which corresponds by transmitting an agreement packet to terminal A after a response delay t_d. The RTT at terminal A is determined by $t_{RT} = 2t_f + t_d$, where the distance can be estimated (with the assumption that t_d is known). However, the propagation delay in indoor applications is typically in the range of nanoseconds, while the t_d can be few microseconds because of the bit synchronization and channel estimation delays [6]. Therefore, the error accumulation over t_d would cause a large error in t_f for even a small clock offset [6].

Many types of radio frequency (RF) signals have been used for indoor ranging and positioning. For example, pulsed ultra-wideband (UWB) signal has been used for high-precise positioning because of its large bandwidth, which can resolve dense multi-path components (MPCs) [2, 13, 14]. Another widely used RF signal for indoor localization is WiFi signal.

2.1.4 Time difference of arrival

The TDOA method estimates the difference of the arrival times of the transmitted signal to any two of the RNs [6]. For example, let t_1, t_2 denotes TOA for two RNs. Since there is no synchronization between the target node and the reference nodes, the transmission time of signal from the TN is unknown. Let d_1 and d_2 denote the distance between the two RNs and the TN. The distance difference between the TN and two RNs can be modeled as:

$$d_{2,1} = d_2 - d_1 = c(t_2 - t_1) \tag{2.3}$$

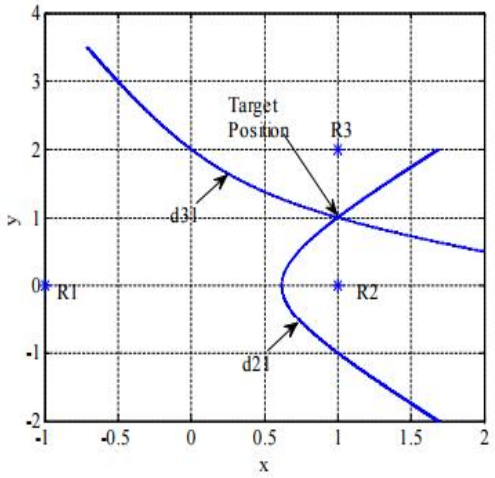

Figure 2.4: Hyperbola theory of TDOA measurement.

The location TN can be determined via the hyperbolas location theory [6, 15], as illustrated in Figure 2.4. The axes x and y in Figure 2.3 is used to form the

grid, with no unit. The hyperbola is a set of points at a constant range-differences from two RNs. In 2-D, TDOA needs at least three RNs to locate the TN. Two hyperbolas can be formed with three RNs, and the intersection of these two hyperbolas is the TN that needs to be estimated. However, TDOA measurement requires precise synchronization between RNs.

2.2 Multipath Channel Model

Multipath propagation is commonly encountered for radio communication. The result is that the transmitted radio signal arrives at the receiving antenna via two or more paths. Multipath can be modeled by using the impulse response of the channel. Consider the ideal case when the transmitted signal is a Dirac delta function, expressed as:

$$x(t) = \delta(t) \tag{2.4}$$

The received signal through a multipath channel can be modeled as [1, 16]:

$$h(t) = \sum_{l=1}^{L_p} h_l \delta(t - \tau_l) \tag{2.5}$$

where h_l and τ_l are the complex amplitude and the time delay of the lth path, respectively, and L_p denotes the total number of paths. The complex amplitude h_l can be further expressed as:

$$h_l = \alpha_l e^{j\phi_l} \tag{2.6}$$

where α_l is the magnitude of the lth path, and ϕ_l is the phase of the lth path. Thus, the received signal can be further expressed as [16]:

$$h(t) = \sum_{l=1}^{L_p} \alpha_l e^{j\phi_l} \delta(t - \tau_l) \tag{2.7}$$

In the presence of time variation of the geometrical reflection conditions, the impulse response is also time varying, for which the related quantities should be written as:

$$\begin{aligned} \alpha_l &= \alpha_l(t) \\ \phi_l &= \phi_l(t) \\ \tau_l &= \tau_l(t) \end{aligned} \tag{2.8}$$

Moreover, Eq. (2.7) can be used to model both LOS and NLOS channels.

The common model of the UWB propagation channel is based on the IEEE 802.15.3a standard model. The IEEE 802.15.3a channel model is developed from

$$h(t) = \sum_{l=1}^{L_p} h_l \delta(t - \tau_l) \tag{2.9}$$

which can be further expressed as [17]:

$$h(t) = X \sum_{l=0}^{L} \sum_{k=0}^{K} \alpha_{l,k} \delta\left(t - T_l - \tau_{l,k}\right) \tag{2.10}$$

where $\alpha_{l,k}$ denotes the multipath gain coefficient of the kth path in the lth cluster, T_l represents the delay of the lth cluster, $\tau_{l,k}$ is the delay of the kth path in the lth

cluster, and X models the log-normal shadowing effects [17]. The IEEE802.15.3a channel has four sub-models:

1. CM1: Based on LOS (0-4m) channel measurements;
2. CM2: Based on NLOS (0-4m) channel measurements;
3. CM3: Based on NLOS (4-10m) channel measurements;
4. CM4: A model that is generated to fit a 25 ns root mean-square (RMS) delay spread to represent an extreme NLOS case;

This thesis will use CM4 model for high-precision and reliable simulation result.

2.3 Time of Arrival Estimators

According to the previous discussion, an accurate ranging result is the foundation of TOA localization. There are several existing methods for TOA estimation. For example, maximum likelihood (ML) and threshold-based methods [13, 18, 19].

2.3.1 Maximum likelihood estimator

The ML estimator aims to find out the propagation delay value τ which maximizes the correlation between the received signal and transmitted signal [20]. The ML estimator can be implemented by using a matched filter (MF) as shown in Figure 2.5.

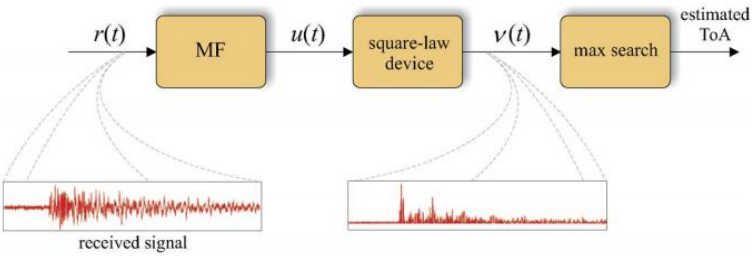

Figure 2.5: The classic MF scheme.

In this figure, $r(t)$ is the received signal, $u(t)$ is the output of the matched filter whose impulse response is denoted by $p(t)$. The square law device is used to maximize the peak value of $u(t)$. The output of the square law device is denoted as $v(t)$.

The main idea of the ML estimator is to use the correlation function to find out the time delay value. Two basic coefficients of ML estimator are the path arrival times $\hat{\tau}$ and their respective amplitudes $\hat{\alpha}$. Let us assume the number of paths L is known. The amplitude and the arrival time vector can be denoted respectively as [20]

$$\hat{\alpha} = [\alpha_1, \alpha_2, ..., \alpha_L]^T \tag{2.11a}$$

$$\hat{\tau} = [\tau_1, \tau_2, ..., \tau_L]^T \tag{2.11b}$$

The ML estimates of $\hat{\tau}$ and $\hat{\alpha}$ can be expressed as [6]

$$\hat{\tau} = \arg\max_{\tau} \chi^T(\tau)\mathbf{R}^{-1}(\tau)\chi(\tau) \tag{2.12a}$$

$$\hat{\alpha} = \mathbf{R}^{-1}(\tau)\chi(\tau) \tag{2.12b}$$

where $\mathbf{R}(\tau)$ is the autocorrelation matrix of $p(t)$ with elements $R_{i,j} = (\tau_i - \tau_j)$, $\chi(\tau)$ is the correlation between the received signal and differently delayed replicas of the transmitted pulse, given by [6]

$$\chi(\tau) = \int_0^T r(t)[p(t-\tau_1)...p(t-\tau_L)]^T dt \tag{2.13}$$

where T is the observation time interval.

ML estimators are known to be asymptotically efficient, that is, they can achieve the Cramer Rao Lower Bounds (CRLB) in the high-SNR region because it can fully recover the transmitted signal after the matched filter. However, it requires the implementation at the Nyquist sampling rate or higher [20]. It leads to a high computational complexity, which limits its applications.

2.3.2 Energy detector based estimator

An energy detector (ED) is easier to implement than the ML estimator since it requires a lower sampling rate than the ML estimator. Although its overall accuracy is not as good as that of the ML estimator, it is easier than the ML estimator to detect the first arrival peak [6]. With the ED, the received signal is illustrated in Figure 2.6.

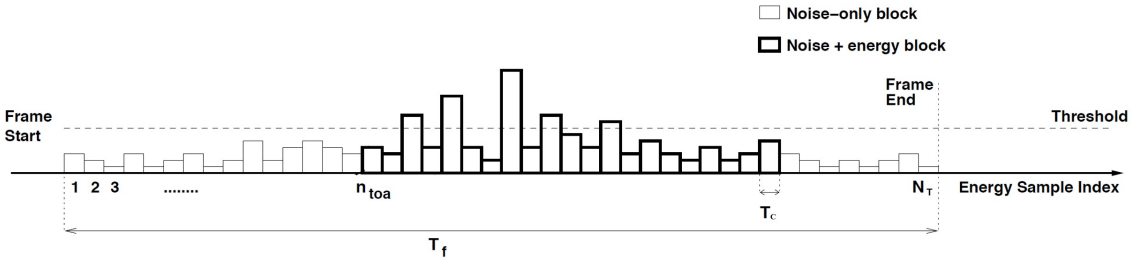

Figure 2.6: The received signal with an energy detector.

In Figure 2.6, T_f is the time duration of a whole frame, T_c is the time duration of each subinterval (i.e., chip interval), N_T is the total number of subintervals, thus $T_f = N_T T_C$. A commonly used ED-based TOA estimator is shown in Figure 2.7.

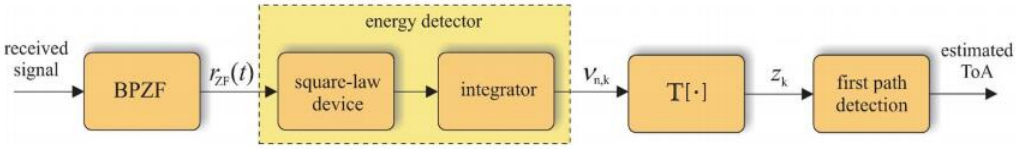

Figure 2.7: The commonly used ED-based estimator.

The received signal is first passed through a bandpass zonal filter (BPZF) with center frequency f_0 and bandwidth W. It is used to eliminate the out-of-band noise. The output of the BPZF can be written as [6]

$$r(t) = s(t) + i(t) + n(t) \tag{2.14}$$

where $i(t)$ is the interfering term depending on the nature of the interference [6],

$s(t)$ can be modeled as [6]

$$s(t) = \sum_{n=0}^{N_t-1} \omega\left(t - c_n T_c - nT_f\right) \tag{2.15}$$

where N_t is the total number of sub-intervals of the received signal, T_c is the chip duration, T_f is the frame duration [6], c_n is a time-hopping coefficient, and the $\omega(t)$ is modeled as [6]

$$\omega(t) = \sqrt{\frac{E_s}{N_t}} \sum_{l=1}^{L} \alpha_l p(t - \tau_l) \tag{2.16}$$

where L is the number of paths, α_l, $l = 1, ..., L$, is the path gains, $\tau_l, l = 1, ..., L$, is the path delay, E_s is the received energy per symbol, N_t is the total number of received sub-intervals, and $p(t)$ is the Dirac Delta function.

Let $\nu_{\mathbf{n},\mathbf{k}}$ be the noise component after energy detection, which is an $N_t \times K$ matrix, where K is the number of samples. The elements of $\nu_{\mathbf{n},\mathbf{k}}$ can be expressed as [6]

$$\nu_{n,k} = \int_{kT_{int}}^{(k+1)T_{int}} |r_n(t)|^2 dt, n = 0, ..., N_t - 1, k = 0, ..., K - 1. \tag{2.17}$$

where $r_n(t)$ is the portion of the signal after the BPZF.

$T[\cdot]$, shown in Figure 2.7, is a linear or nonlinear transformation, outputting a signal $z[n]$, which is used to detect the first path [6]. $z[n]$ is modeled as:

$$z[n] = T\left[\nu_{n,k}\right], k = 0, ..., K - 1. \tag{2.18}$$

The TOA can be determined by finding out the first arrival subintervals (i.e., the exact number n in Figure 2.6, $n = 1, ..., N_T$). The ED-based estimator will be the focus of this research because of its simplicity. The goal is to find the arrival time slot of the first peak by setting a proper threshold value related to the SNR at the receiver.

Chapter 3: Threshold Selection Based on SNR

3.1 Motivation

Current techniques have not established the relationship for the threshold selection and the SNR. An adaptive threshold for channels with varying noise levels and signal levels will improve TOA estimate accuracy. There are extensive literature studying how to improve the accuracy of timing detection in the TOA measurement through an adaptive threshold selection [4, 5, 21, 22]. However, most of them either assume SNR value is known or neglect the SNR value. A fixed threshold value is set by observing a large set of collected received data in [4]. An adaptive normalized threshold method is proposed in [5], which takes into consideration of the minimum and the maximum values in the received signal. Both of these two threshold selection methods did not consider SNR.

The SNR at the receiver will affect received signal characteristics. SNR is a measure used to compare the level of a desired signal to the level of background noise. The definition of SNR is expressed as:

$$SNR = \frac{\sigma^2_{Signal}}{\sigma^2_{Noise}} \tag{3.1}$$

where σ_{Noise} and σ_{Signal} are the standard deviations of noise signal and transmitted signal, respectively.

According to [23], the expression for the threshold can be expressed as:

$$\xi = \sigma_n \cdot Q^{-1}(P_{fa}) + \mu_n, \tag{3.2}$$

where σ_n represents the noise variance, $Q^{-1}(\cdot)$ represents the inverse Q-function, P_{fa} denotes the false alarm probability, and μ_n is the mean value of the noise signal.

Furthermore, the false alarm probability can be expressed as [24]:

$$P_{fa} = n_p \cdot \frac{\log 2}{n_{fa}} \tag{3.3}$$

where n_p is the number of integrated pulses, which represents the number of pulses in one detected symbol, n_{fa} is false alarm number, defined as the number of pinpoints exceeding the threshold value in the received signal.

The research in [22, 24] substitutes the false alarm probability P_{fa} into the original threshold expression. It turns out that the threshold expression can be expressed as:

$$\xi = \sigma_{noise} \cdot Q^{-1}\left(\frac{\log 2}{n_{fa}}\right) + \mu_{noise} \tag{3.4}$$

Eq. (3.1) and Eq. (3.4) show that the SNR has a significant impact on the threshold value selection. Thus, a new comprehensive threshold-selection method based on the SNR is needed.

3.2 Theory Development

The threshold based estimation can be done via three common algorithms: maximum energy selection (MES), maximum energy selection with search-back (MES-SB), and threshold comparison (TC).

3.2.1 Maximum energy selection

MES is the simplest way to estimate TOA among these three algorithms [4, 6]. It mainly detects the strongest energy block from the beginning of the time frame, which can be evaluated as [4]:

$$\begin{aligned} \widehat{\tau} &= \left[\arg \max_{1 \le n \le N_b} z[n] \right] T_b \\ &= n_{max} T_c \end{aligned} \tag{3.5}$$

where n_{max} represents the block having the largest energy, T_b is the time duration of a block, and N_b is the total number of block per frame. It means that the TOA is the largest energy block's corresponding time bin, as shown in Figure 3.1.

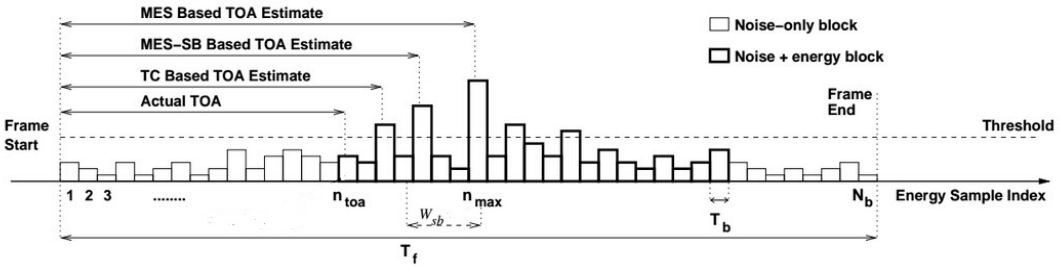

Figure 3.1: Algorithms for threshold-based TOA estimation.

However, this method cannot give an accurate estimate since the largest energy block in many cases may not be the leading energy block [4]. Additionally, its performance decreases as N_b increases because as N_b increases the probability that a noise block become the maximum-energy block increases.

3.2.2 Maximum energy selection with search-back

The MES-SB is an improved version of the MES [4]. The MES-SB is based on the detection of the largest sample and a search-back procedure. The search begins from the largest sample in the signal $z[n]$, with index n_{max}. $z[n]$ is the signal after a linear or nonlinear transformation (as shown in Figure 2.7). The search proceeds element by element backward in a window of length W_{sb} until the sample under test goes below the threshold ξ. The size of W_{sb} is based on the channel statistics.

The TOA estimate is given as:

$$\widehat{\tau}_{MES-SB} = [\min n | \widetilde{z}[n] < \xi + n_{max} - W_{sb} - 1]T_b \tag{3.6}$$

where $\widetilde{z}[n] = [z[n_{max} - W_{sb}]z[n_{max} - W_{sb} + 1]...z[n_{max}]]$.

An open issue of this method is to decide of the size of W_{sb}. A proper size depends primarily on the accuracy of channel estimator [6].

3.2.3 Threshold comparison

The TC criterion is based on the timing detection of the first arrival peak, and hence the estimated TOA, through comparing each element of $z[n]$ within the observation interval T_f to a threshold. The threshold can be found by using the existing fixed threshold value method or the adaptive threshold selection method. The time of the first block that exceeds the threshold is the estimated TOA, which is expressed as:

$$\widehat{\tau}_{TC} = \min\{n | z[n] > \xi\} \cdot T_b. \tag{3.7}$$

where ξ is the threshold.

A proper threshold value should be designed depending on the received signal characteristics, the operating condition, and the channel characteristics. The fixed threshold method is designed based on the evaluation of the probability of early

detection P_{ed}, which is modeled as [4, 6]

$$P_{ed} = 1 + \frac{(1 - q_0)^{n_{toa}} - 1}{n_{toa} q_0} \tag{3.8}$$

where n_{toa} is the actual first arrival peak (shown in Figure 3.1). q_0 is a variable built according to the characteristic of the centralized chi-square distribution with M degree of freedom, which is given as [6]

$$q_0 = \exp(-TNR) \sum_{i=0}^{M/2-1} \frac{TNR^i}{i!} \tag{3.9}$$

where $TNR = \xi / N_0$, N_0 denotes the noise power; $M = 2N_b T_f W$, N_b is the total number of subintervals, T_f is the time duration of a frame, and W is the bandwidth of the transmitted signal [6].

Eqs. (3.8) and (3.9) show that the threshold ξ can be determined through TNR, corresponding to a target value of P_{ed}. However, this design of the threshold value depends neither on the received signal characteristic nor on the channel characteristics.

Based on the fixed threshold selection method, the work in [4] proposes to use the normalized adaptive threshold, where the threshold value ξ is based on the received signal statistics. The normalized adaptive threshold value can be evaluated by using the minimum and maximum energy sample values, which is expressed as:

$$\xi_{norm} = \frac{\xi - \min\{z[n]\}}{\max\{z[n]\} - \min\{z[n]\}} \tag{3.10}$$

where ξ_{norm} is the normalized adaptive threshold value.

The criterion of the normalized adaptive threshold selection method can be illustrated through Figure 3.2. However, this method does not consider the channel characteristics or the SNR value at the receiver.

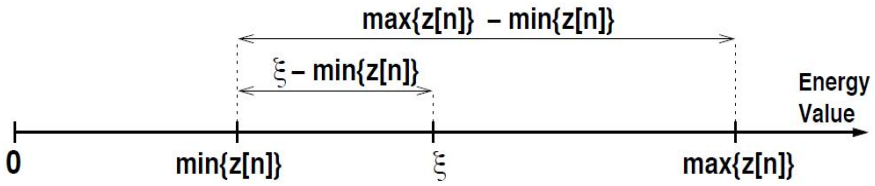

Figure 3.2: Illustration of the adaptive normalized threshold selection method.

3.3 Adaptive TOA Threshold Selection Method Based on Channel SNR

In this section, an adaptive threshold selection method is proposed. The proposed method is based on two assumptions:

- There is a channel estimator which can estimate the relatively accurate SNR value at the receiver.
- The transmitter and receiver are synchronized.

According to the sampling criterion of the ED-based estimator, the received signal after sampling is shown in Figure 3.3. N_T is the total number of subintervals, which is the sample index as well; n_{toa} is the index of the true first arrival peak; T_f is the frame duration; T_c is the time duration of a subinterval. The frame duration

T_f is determined by the transmitted signal structure. The frame starting point is decided by observing the figures of the transmitted and received signals. The total number of received pulses will be set as N_p, which is the size of the receiving window W_s, that is, the number of pulses that the receiver can store per process.

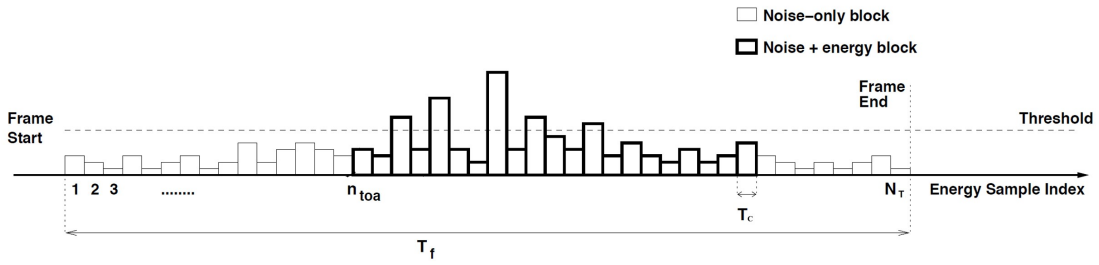

Figure 3.3: Received signal after sampling.

With the assumption of that the channel estimator is accurate, the SNR value at the receiver can be evaluated. After evaluating the received power E_s, which is the sum of the received signal power and noise power, the power of the received signal $E_i, (i = 1, 2, ..., N_p)$ can be calculated. The process can be expressed as:

$$\begin{aligned} \frac{E_i}{N_0} &= SNR \\ E_i + N_0 &= E_s \end{aligned} \tag{3.11}$$

The peak values $A_p(p = 1, 2, ..., N_p)$ of each received pulse can be calculated after knowing the value of E_i. Thus, the minimum and the maximum peak values among the N_p pulses can be obtained, respectively, denoted as A_{min} and A_{max}.

The work in [21] uses the fixed threshold method to find a threshold value ξ_1

by setting an acceptable P_{ed} value. The threshold value ξ_1 can be used to detect the exact position of the first arrival peak in one received pulse, denoted as n_{toa}. A mean absolute error (MAE) is applied to analyze the fixed threshold method in [21], which can be modeled as [4]

$$e_{abs} = \sum_{n=1}^{N_T} P_D(n) \times |n - n_{toa}| \tag{3.12}$$

where $P_D(n)$ is the probability of detecting an arbitrary block n, which can be expressed as [4]

$$P_D(n) = \left[\prod_{n=1}^{N_T - 1} P(z[n] < \xi) \right] \times P\left(z[n] > \xi\right) \tag{3.13}$$

where $z[n]$ has a central chi-square distribution for $n = 1, 2, ..., n_{toa} - 1$, and non-central chi-square distribution for $n = n_{toa}$ [4]. By applying the MAE algorithm (Eqs. (3.12)-(3.13)) to this thesis, MAE could be calculated, denoted as e_{bias} in this thesis. The n_{toa} and e_{bias} values are set as the reference parameters in this proposed method.

The threshold selection loop can be named as area searching (AS). The average value between A_{min} and A_{max} is set as the first threshold value TH_{11} for AS, expressed as:

$$TH_{11} = \frac{A_{min} + A_{max}}{2}. \tag{3.14}$$

The area between A_{min} and A_{max} has been separated into two areas by TH_{11}. Area 1 is from A_{min} to TH_{11}, and the rest is area 2. The indexes for the first arrival

peak can be found by using the threshold value TH_{11}, which can be obtained by an $N_p \times 1$ vector, denoted by $\mathbf{n_{toa11}}$. A total of N_p true n_{toa} values are used to form the reference vector with the same dimension as $\mathbf{n_{toa11}}$, named $\mathbf{n_{toa}}$. The vector $\mathbf{n_{toa11}}$ will be compared with the reference vector $\mathbf{n_{toa}}$. A bias vector $\mathbf{e_b}$ can be found by comparing these two vectors, expressed as:

$$\mathbf{e_b} = \mathbf{n_{toa11}} - \mathbf{n_{toa}}. \tag{3.15}$$

An average bias value e_{b1} can be found by calculating the mean value of the absolute value of $\mathbf{e_b}$. If $e_{b1} > e_{bias}$, then the threshold value TH_{11} will be compared to the corresponding amplitude of n_{toa}, named $A(n_{toa})$, to decide which searching area to conclude in. If $A(n_{toa}) - TH_{11} < 0$, it means the threshold value needs to be decreased. Thus, the searching area concludes in area 1. The next re-set threshold value TH_{12} will be the average value between A_{min} and TH_{11}, expressed as:

$$\begin{aligned} TH_{12} &= \frac{A_{min} + TH_{11}}{2} \\ &= \frac{A_{min} + \frac{A_{min}+A_{max}}{2}}{2}. \end{aligned} \tag{3.16}$$

If $A(n_{toa}) - TH_{11} > 0$, it means the threshold value needs to be increased. Thus, the searching area concludes in area 2. The next re-set threshold value TH_{12} will be the average value between TH_{11} and A_{max}, expressed as:

$$\begin{aligned} TH_{12} &= \frac{TH_{11} + A_{max}}{2} \\ &= \frac{\frac{A_{min}+A_{max}}{2} + A_{max}}{2}. \end{aligned} \tag{3.17}$$

The AS will be kept implementing till e_{b1} satisfies $e_{b1} \leq e_{bias}$. $TH_{1i}, i = 1, 2, ...$ at the stopping time will be the final threshold value TH.

The process illustrated above is used to find a threshold value in one pulse. The remaining $N_p - 1$ pulses will have the same process as the first pulse. The coefficients setting will be introduced in the simulation part. Also, the simulation result for the proposed method will be introduced.

Chapter 4: Simulation

4.1 Simulation Setting

The simulated time-of-arrival system can be separated into four major parts: the transmitter, the channel, the receiver, and the estimator blocks, as shown in Figure 4.1.

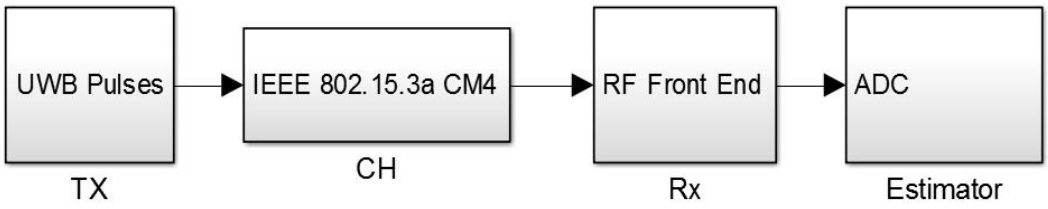

Figure 4.1: System block diagram.

TX is the transmitter block; it generates and transmits a wideband signal (for example, pulsed ultra wideband signal). CH is the channel block; it creates the multipath transmission environment. RX is the receiver block; it receives the transmitted signal. Also, the filters in the receiver are assumed to filter out the interfering signals. The estimator block implements the sampling process and the proposed algorithm. Also, the ADC in the estimator block is used to transform the analog signal to digital signal.

4.1.1 Transmission block

The detailed construction of the transmission block is shown in Figure 4.2, where a pulsed ultra wideband (UWB) signal is used as an example. The UWB sequence block in Figure 4.2, a connecting block between Simulink and Matlab, is used to generate the ultra wideband signal by using the generated math function and the corresponding data; the bernoulli binary generator is used to generate a random sequence; the product block is used to produce the on-off keying (OOK) modulation.

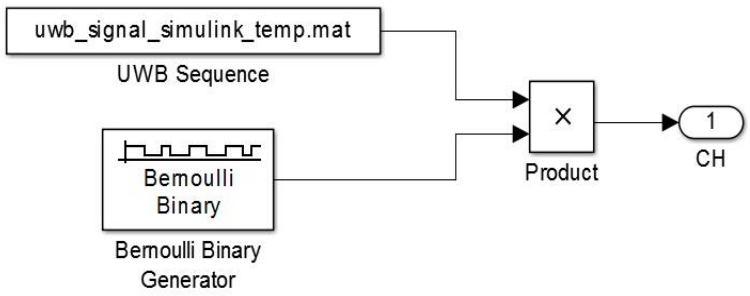

Figure 4.2: Construction of the transmitter.

The UWB sequence block is used because Simulink does not have an ultra wideband signal generator. The information sent from Matlab to the UWB sequence block is the generated Gaussian-like pulse UWB signal. The Gaussian-like pulse is expressed as:

$$G(\tau) = \left(1 - 4\pi \times (\frac{t}{\tau})^2\right) \times \exp\left(-2\pi \times (\frac{t}{\tau})^2\right), \tag{4.1}$$

where τ is the input for the Gaussian-like pulse, set as 0.35 in the simulation, which

is used to define the magnitude of the pulse; t gives the pulse's segment numbers in the time domain, which is from -50 to 50, with a step size of 0.05.

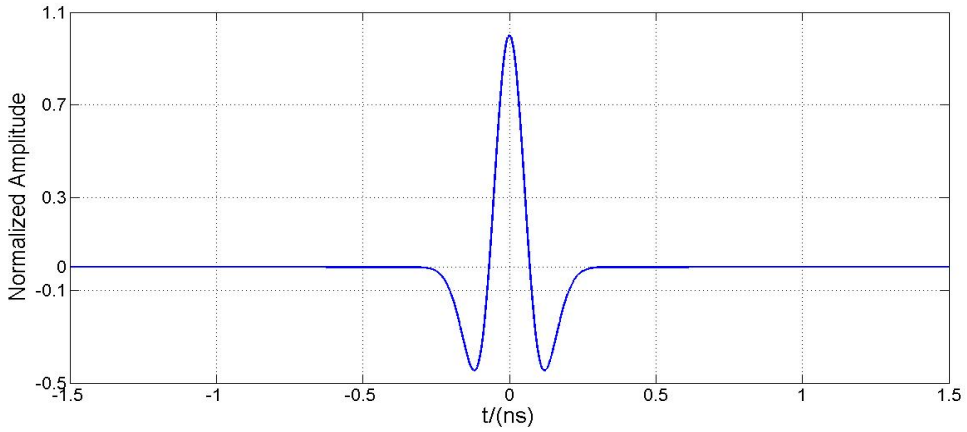

Figure 4.3: A single Gaussian-like pulse.

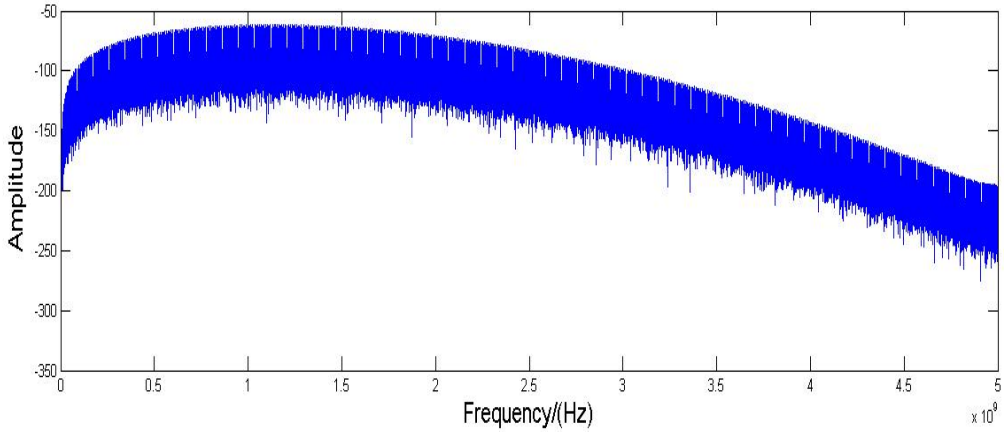

Figure 4.4: Fourier transform of transmitted signal.

The section duration for T_f is 70ns. Figure 4.3 shows the zoomed-in part of

the Gaussian-like pulse, and Figure 4.4 shows the frequency domain transmitted signal, obtained by taking the Fourier transform of the time-domain signal, and is expressed as:

$$F(f) = \int_{-\infty}^{\infty} f(t)e^{-2\pi tf}dt. \tag{4.2}$$

where $G(\tau)$ in Eq. (4.1) is the transmitted signal $f(t)$.

The size of the receiving window W_s, introduced in the proposed algorithm, is $N_p = 20$. Thus, 20 Gaussian like pulses (with the same expression as Eq. (4.1)) are put together having the same period and the same section time T_f. In terms of modulation, OOK can be modeled as:

$$s(t) = A(t)g(t) \tag{4.3}$$

where $s(t)$ is the modulated signal; $A(t)$ is the key for OOK modulation, whose value is either 0 or 1; $g(t)$ is the ultra wideband signal.

4.1.2 Channel block

The construction of the channel block is shown in Figure 4.5. The whole channel block in Simulink can be shown in Figure 4.6, which is provided in [25]. It can simulate the multipath transmission environment. This channel block can create the IEEE 802.15.3a line of sight (LOS) and the non-line of sight (NLOS) environments. In order to increase the accuracy and the reliability of the simulation result, an ad-

ditional Gaussian noise generator is applied. An example of the output of channel block, including the Gaussian noise in the frequency domain is shown in Figure 4.7.

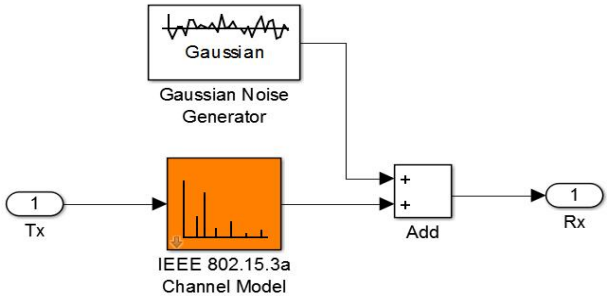

Figure 4.5: Construction of the channel block.

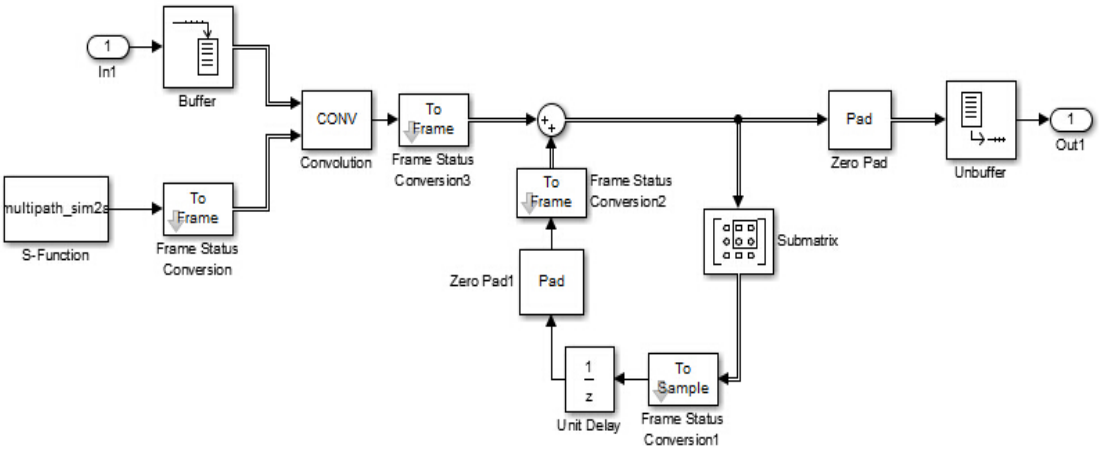

Figure 4.6: IEEE 802.15.3a channel block.

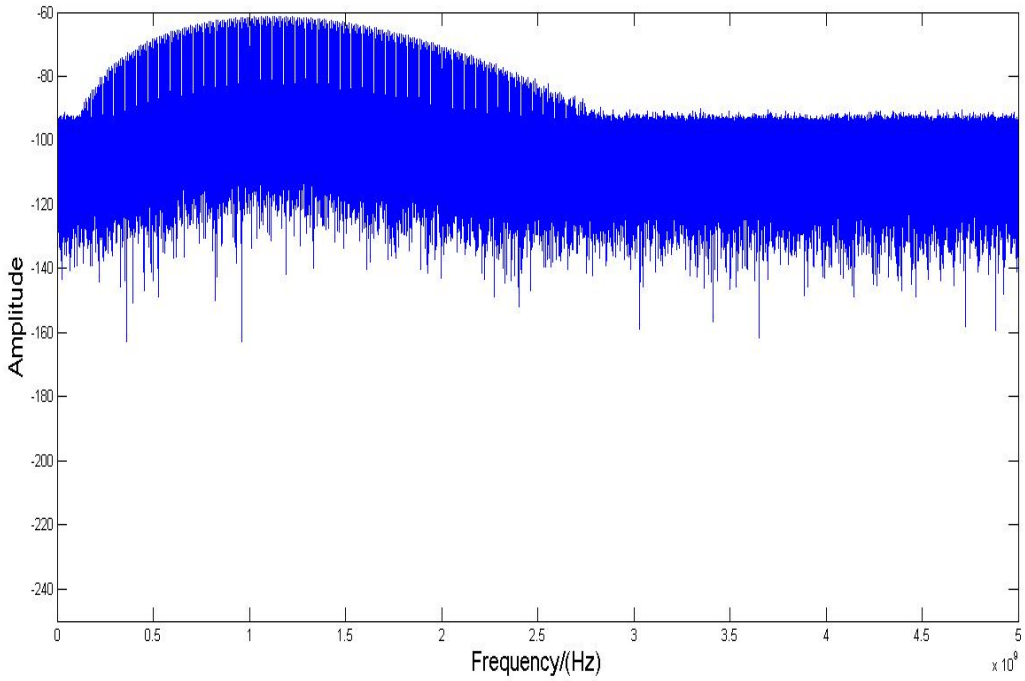

Figure 4.7: Transmitted signal after channel.

Since the channel block has an additional Gaussian noise generator, it can be used to control the SNR value by changing the noise variance in the noise generator. In this simulation, the noise variance for the low SNR region is set to $[1.5 \times 10^{-4}, 15 \times 10^{-4}]$, which corresponds on SNR range of 14dB to 21dB. The noise variance $[1.5 \times 10^{-5}, 15 \times 10^{-5}]$ corresponds the high SNR region, from 23dB to 32dB.

4.1.3 Receiver block

The construction of the receiver block is shown in Figure 4.8. The signal first passes through a band pass filter (BPF), which is used to eliminate the out band noise signal. The bandwidth of the BPF is set to be 1GHz, from 0.9GHz to 1.9GHz. The signal then arrives at the low noise amplifier (LNA), which is used to amplify the signal. In general cases, it is required to have a 20dB bent, 10 times of gain. The signal will then pass through a square function and an integrator after the LNA. The square function is the square law device, which is used to amplify the peak value of the signal for the algorithm in the estimator block. The integrator is a low pass filter, which connects the square law device as an energy detector. The stop frequency is set as 1.9GHz, and the pass frequency is set as 1GHz in the LPF. The effects of each sub-block in the receiver block presented above are shown in Figure 4.9.

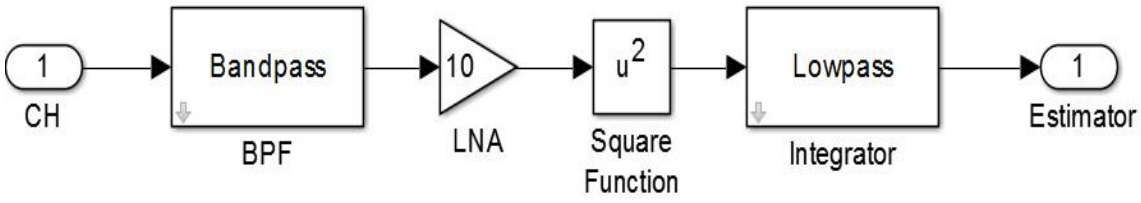

Figure 4.8: Receiver blocks in Simulink.

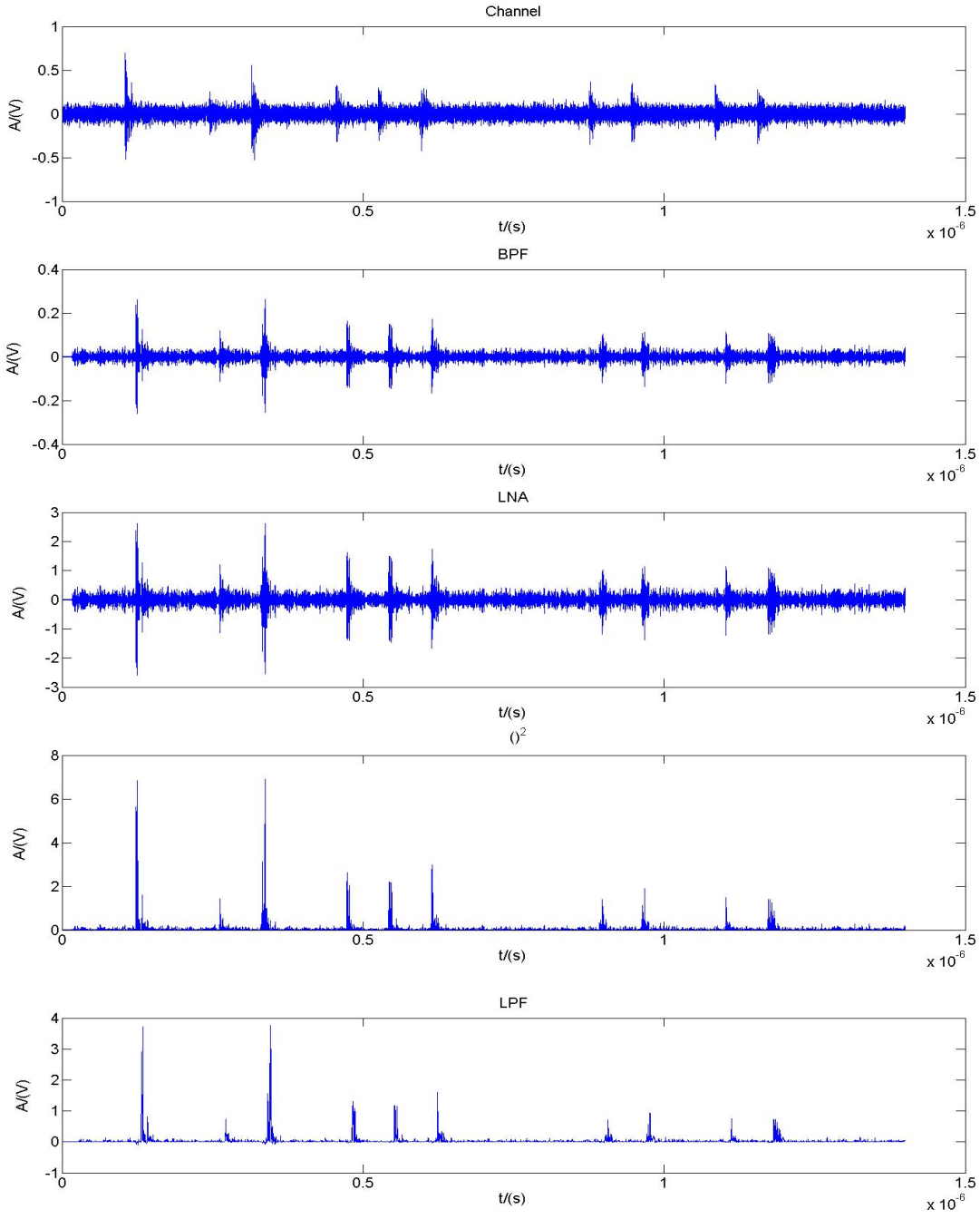

Figure 4.9: Signal waveform at various points of the receiver.

4.1.4 Estimator block

The estimator block is used to sample the received signal, and to implement the proposed algorithm after sampling. The sub-sampled signal is shown in Figure 4.10, where the upper figure is the whole sub-sampled received signal, and the lower figure is one section of the sub-sampled received signal. The proposed algorithm is implemented based on the sub-sampled received signal.

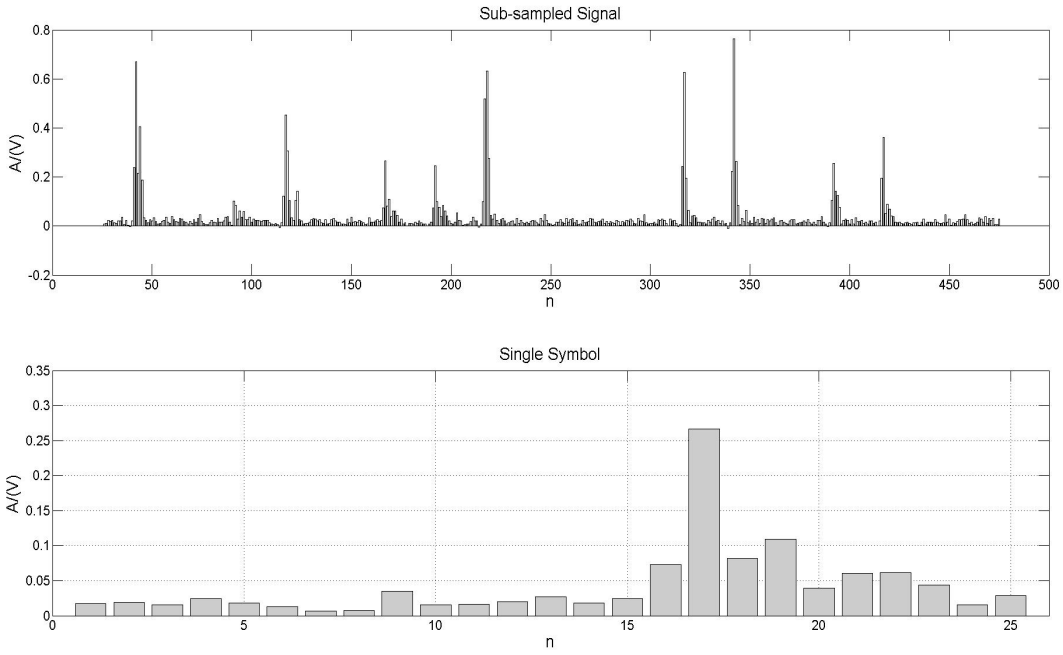

Figure 4.10: Sub-sampled received signal.

4.2 Result and Analysis

This section analyzes the results of the proposed algorithm in two areas: one is the relationship between the threshold value and the SNR; the second is the ranging error performances with the proposed algorithm.

4.2.1 Relationship between the threshold value and the SNR value at the receiver

Here we focus on assessing how SNR at the receiver affects the threshold value. The SNR value at the receiver is divided into two regions in this simulation to have a clearly observation, which are the low SNR value region (the SNR value is from approximately 14dB to about 21dB), and the high SNR value region (the SNR value between 23dB and 31dB).

The relationship between the threshold and the SNR in low SNR region is shown in Figure 4.11. It can be seen that the threshold value increases as the SNR value decreases. A decreasing SNR means that the noise power increases while the power of the received signal remains the same. The threshold value is optimized to minimize the false alarm probability, which has been introduced in Chapter 3. Thus, the decrease of the SNR leads to an increase of the threshold value in the low-SNR region. The relationship between the threshold and SNR in the high SNR region is shown in Figure 4.12, which shows that the threshold value also increases as the SNR value decreases.

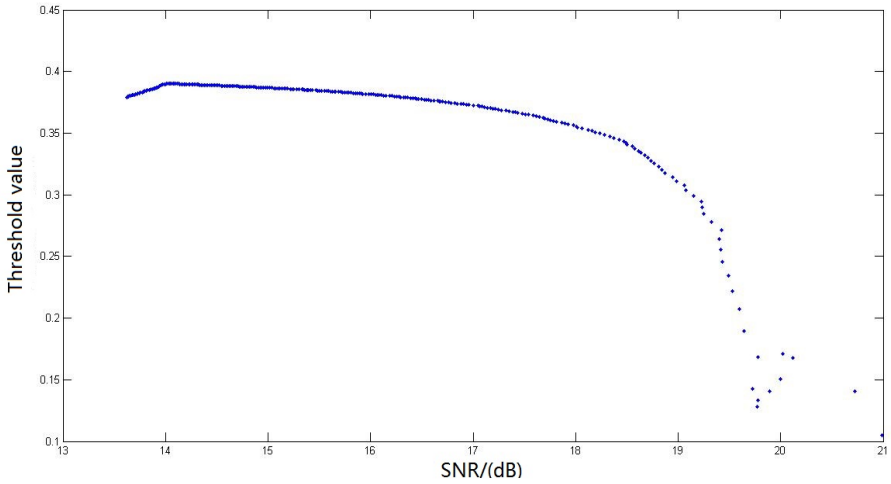

Figure 4.11: The threshold in the low-SNR region.

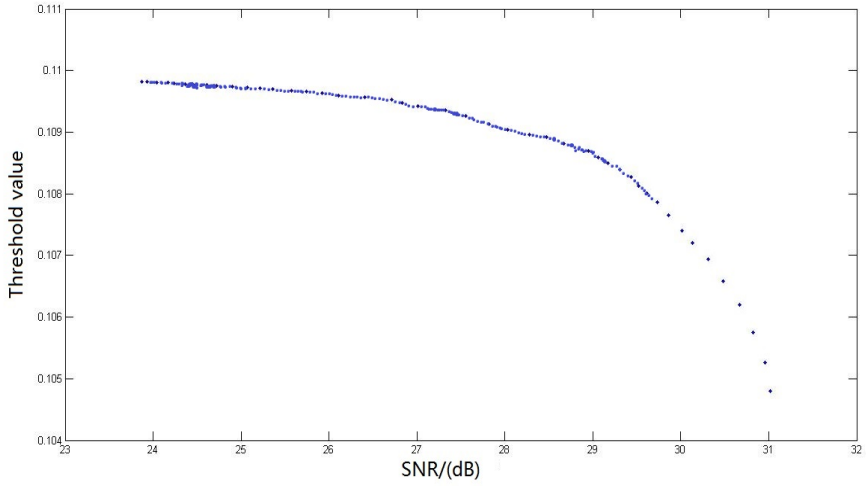

Figure 4.12: The threshold in the high-SNR region.

From the above two figures, we arrive at the following conclusion: the relationship between the threshold and the SNR value is that the threshold value would increase as the SNR value decreases.

Next we describe the process of determining an approximate mathematical expression to represent the above relationship. Specifically, we establish the relationship between the SNR value and the threshold value by using the expressions of the probability of detection and the probability of the false alarm [26, 27]. The probability of detection can be expressed as [26]

$$P_D = 0.5 \times erfc(\sqrt{-\ln P_{fa}} - \sqrt{SNR + 0.5}) \tag{4.4}$$

where $erfc(\cdot)$ is the complementary error function, P_{fa} is the false alarm probability. The complementary error function $erfc(\cdot)$ can be expressed as:

$$erfc(x) = 1 - \frac{2}{\sqrt{\pi}} \int_0^x e^{-v^2} dv. \tag{4.5}$$

According to [27], the probability of false alarm, P_{fa}, can be expressed as:

$$P_{fa} = 1 - \Gamma(\frac{V_T}{\sqrt{n_p}}, n_p - 1) \tag{4.6}$$

where V_T is the threshold value, $\Gamma(\cdot)$ is the gamma function, and n_p is the total integrated numbers of subintervals. The gamma function is expressed as [24]

$$\Gamma(s, x) = \int_x^\infty t^{s-1} e^{-t} dt \tag{4.7}$$

where s is $\frac{V_T}{\sqrt{n_p}}$ in Eq. (4.6) and x is $n_p - 1$ in Eq. (4.6).

From Eqs. (4.4)-(4.7), we conjecture that the relationship between the threshold value and the SNR could be approximated by using either the exponential function or the Gaussian function. Firstly, we make an attempt to fit the Threshold-SNR curve using an exponential function. It turns out that a two-term exponential function expressed as

$$f(x) = a \cdot e^{(b \cdot x)} + c \cdot e^{(d \cdot x)} \tag{4.8}$$

fits the SNR-threshold results well. In Eq. (4.8), the curve coefficients a, b, c, d could be could be determined by using the simulation results. Figure 4.13 shows the fitting results: the upper figure is the curve for the low SNR value region, and the lower figure is the curve for the high SNR value region.

Another attempt is to use the following three-term Gaussian function

$$f(x) = a_1 e^{-(\frac{(x-b_1)}{c_1})^2} + a_2 e^{-(\frac{(x-b_2)}{c_2})^2} + a_3 e^{-(\frac{(x-b_3)}{c_3})^2} \tag{4.9}$$

to fit the SNR-threshold relationship. The curve coefficients a_i, b_i, c_i, $i = 1, 2, 3$, again can be determined by using the threshold-SNR simulation results. Compared to the Gaussian fitting, the exponential fitting results is a better match.

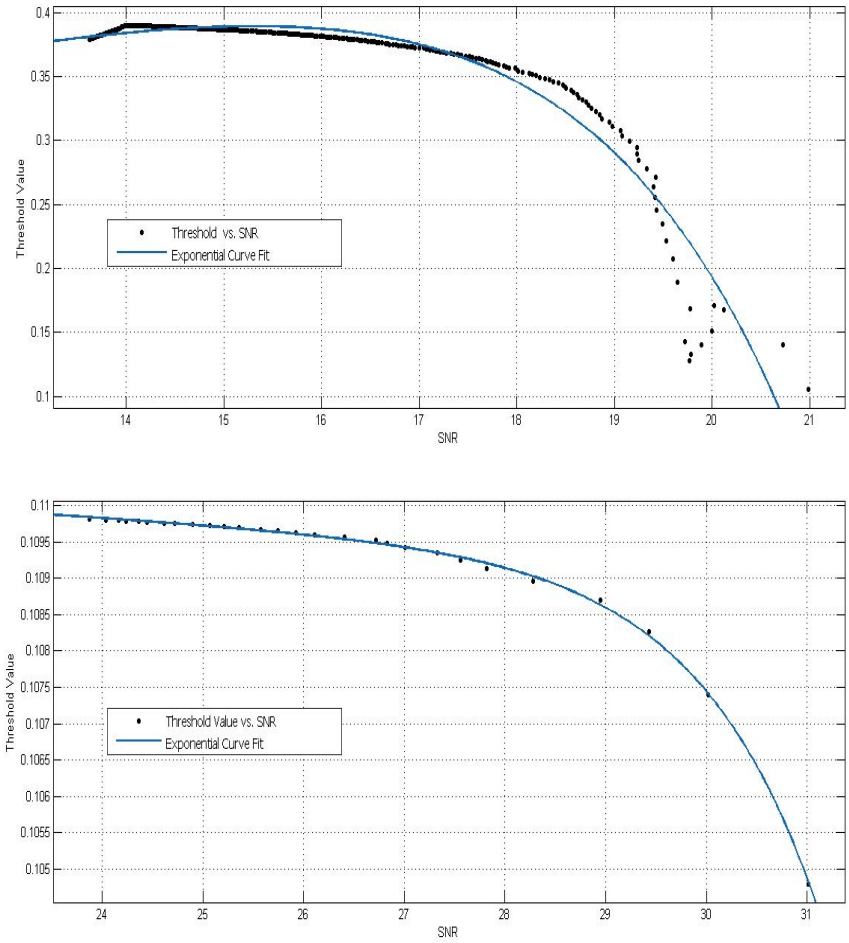

Figure 4.13: Two-term exponential curve fitting result

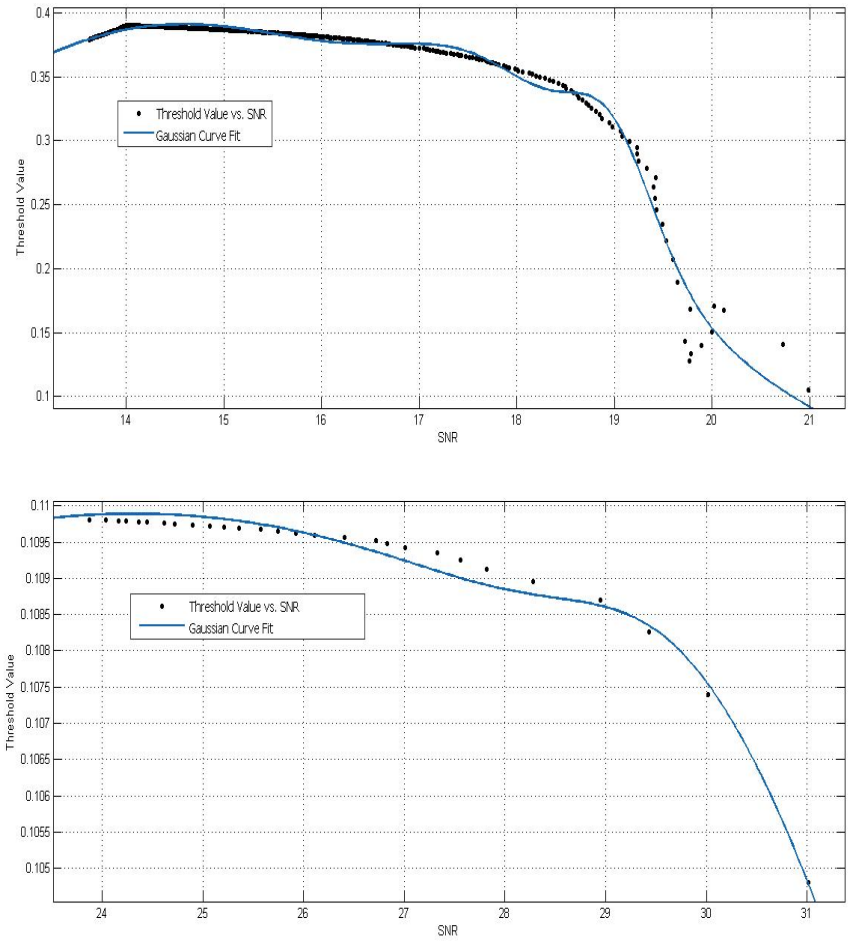

Figure 4.14: Three-term Gaussian curve fitting result

4.2.2 Ranging error performance

This section presents the ranging error performance for the proposed algorithm. The performance is evaluated by calculating the mean absolute error (MAE), which is the average difference between the estimated first arrival peak and true first

arrival peak. Ranging error is expressed as:

$$\text{Ranging error} = e_M \cdot T_c \cdot c \tag{4.10}$$

where e_M is the MAE, T_c is the sub-interval duration, and c is the speed of light.

The method to find the true indexes of the first arrival peak is presented in the proposed algorithm. After getting the true first arrival peak's indexes, the simulation takes 75 different SNR values ranging from 21dB to 31dB to record the estimated indexes. The estimated indexes and true indexes can be used to calculate the MAE. The following table shows the matrix of the mean values of MAEs at 75 different SNR values, in which the first row are the pulse indexes and the second row are the corresponding MAE values.

Pulse	1	3	4	6	7	8	12	13	15	16
MAE	1.107	0.467	0.873	0.433	0.460	0.413	0.420	0.433	0.927	0.433

Table 4.1: MAEs at 75 different SNR values

The following table shows the ranging error values, where the first row means the index of the pulses, and the second row are the ranging error values (the unit is meter).

Pulse	1	3	4	6	7	8	12	13	15	16
Ranging error	0.92	0.39	0.73	0.36	0.38	0.35	0.35	0.36	0.77	0.36

Table 4.2: Ranging error values at 75 different SNR values

The mean value of MAEs is 0.597, which means the ranging error is about 0.50m. During the process of evaluating the MAE, there is a concern that the proposed threshold algorithm might result in a relatively low-accuracy detection of the first arrival peak when the SNR value is lower than a certain value. The following table shows the estimated indexes (shown as 'Block No.' in the table) of the first arrival peak in low-SNR region, 13dB-21dB.

Pulse No.	1	2	3	4	5	6	7	8	9	10	11	12	13	14	15	16
Block No.	17	0	17	17	24	19	18	18	0	0	0	16	17	0	17	20

Table 4.3: The estimated indexes of the first arrival peak in low-SNR region

The average difference between the estimated indexes and true indexes is 1.1. The ranging error under 13dB-21dB is 0.924m, which is much larger than 0.50m (the mean ranging error for 75 SNR values). Such result is expected though.

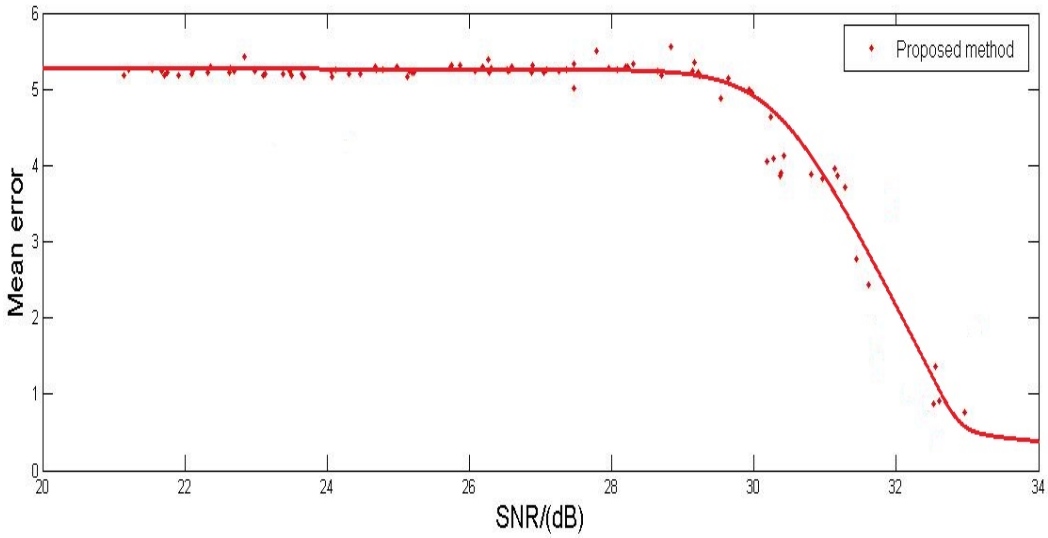

Figure 4.15: Ranging error performance of the proposed algorithm.

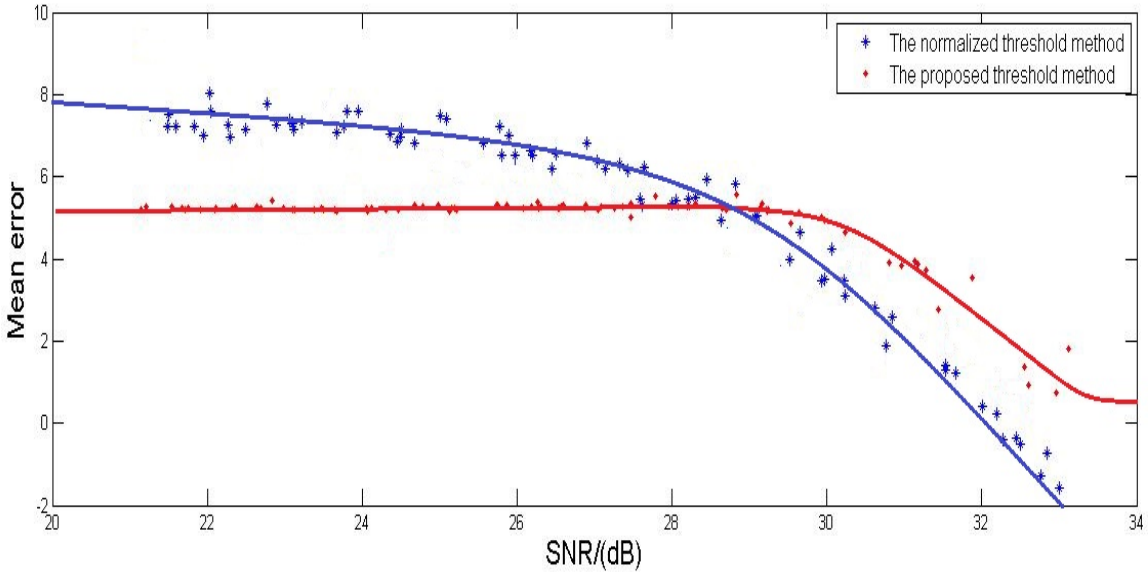

Figure 4.16: Ranging error performance of the proposed algorithm.

The relationship between the mean error and the SNR is presented in Figure 4.15. It shows that the mean error decreases as the SNR value increases. Also, it shows that the threshold has a relatively stable value after 33dB. Figure 4.16 shows the comparison of the mean error between using the normalized threshold method and the proposed threshold method. Compared to the normalized threshold value, the proposed threshold method gains a higher accuracy in the region 21dB to 29dB. The normalized threshold method performs better in the range of 29dB to 32dB.

Chapter 5: Conclusion and Future Work

5.1 Conclusion

This thesis focus on finding a new threshold selection method, which takes SNR into consideration, to improve the accuracy of indoor positioning. Also, it focus on modeling the relationship between the threshold and SNR. Setting a proper threshold based on the received SNR is important for achieving highest positioning accuracy possible. However, existing methods that use a fixed threshold or the normalized threshold do not take SNR into consideration. We have developed an adaptive threshold method that optimizes its value based on SNR. We evaluate the performance of the proposed threshold method by calculating the MAE values, the ranging error values at different SNR values, and compare its performance with that of the normalized threshold method. It is observed that the proposed method performs better than the normalized threshold method. We also developed a two-term exponential function that establishes the relationship between the threshold and SNR, allowing the relationship to be conveniently used in practical systems.

5.2 Future Work

Firstly, an adaptive threshold algorithm to improve the accuracy of the ToA estimation result needs to be developed for operation in the low-SNR region. Secondly,

the Gaussian range-error (noise) model is commonly used in the literature, but such model has not been proven to be suitable for all practical cases. A comprehensive noise model will be valuable. Thirdly, a model relates the SNR at the receiver and the ToA estimation error will be very useful.

Bibliography

[1] C. Falsi, D. Dardari, L. Mucchi, and M. Win, "Time of arrival estimation for uwb localizers in realistic environments," *EURASIP Journal on Applied Signal Processing*, vol. 2006, pp. 152–152, 2006.

[2] D. Dardari, C. Chong, and M. Win, "Analysis of threshold-based toa estimators in uwb channels," in *Proceedings of 14th European Signal Processing Conference (EUSIPCO06)*, 2006.

[3] I. Guvenc and Z. Sahinoglu, "Threshold selection for uwb toa estimation based on kurtosis analysis," *Communications Letters, IEEE*, vol. 9, no. 12, pp. 1025–1027, Dec 2005.

[4] I. Guvenc, "Low complexity toa estimation for impulse radio uwb systems," *IEEE Journal on Selected Areas in communication*, 2005.

[5] I. Guvenc and Z. Sahinoglu, "Threshold-based toa estimation for impulse radio uwb systems," in *Ultra-Wideband, 2005. ICU 2005. 2005 IEEE International Conference on*, Sept 2005, pp. 420–425.

[6] D. Dardari, A. Conti, U. Ferner, A. Giorgetti, and M. Win, "Ranging with ultrawide bandwidth signals in multipath environments," *Proceedings of the IEEE*, vol. 97, no. 2, pp. 404–426, Feb 2009.

[7] I. Guvenc and C. Chong, "A survey on toa based wireless localization and nlos mitigation techniques," *Communications Surveys Tutorials, IEEE*, vol. 11, no. 3, pp. 107–124, rd 2009.

[8] N. Alsindi, B. Alavi, and K. Pahlavan, "Empirical pathloss model for indoor geolocation using uwb measurements," *Electronics Letters*, vol. 43, no. 7, pp. 370–372, March 2007.

[9] R. Peng and M. Sichitiu, "Angle of arrival localization for wireless sensor networks," in *Sensor and Ad Hoc Communications and Networks, 2006. SECON '06. 2006 3rd Annual IEEE Communications Society on*, vol. 1, Sept 2006, pp. 374–382.

[10] P. Brida, J. Machaj, J. Benikovsky, and J. Duha, "A new complex angle of arrival location method for ad hoc networks," in *Positioning Navigation and Communication (WPNC), 2010 7th Workshop on*, March 2010, pp. 284–290.

[11] I. Guvenc, Z. Sahinoglu, and P. Orlik, "Toa estimation for ir-uwb systems with different transceiver types," *Microwave Theory and Techniques, IEEE Transactions on*, vol. 54, no. 4, pp. 1876–1886, June 2006.

[12] T. Gigl, P. Meissner, J. Preishuber, and K. Witrisal, "Ultra-wideband system-level simulator for positioning and tracking (u-spot)," in *Indoor Positioning and Indoor Navigation (IPIN), 2010 International Conference on*, Sept 2010, pp. 1–9.

[13] D. Dardari, C. Chong, and M. Win, "Threshold-based time-of-arrival estimators in uwb dense multipath channels," *Communications, IEEE Transactions on*, vol. 56, no. 8, pp. 1366–1378, August 2008.

[14] I. Guvenc and Z. Sahinoglu, "Low complexity toa estimation for impulse radio uwb systems," *Mitsubishi Electric Research Labs*, 2005.

[15] H. Elkamchouchi and M. Mofeed, "Direction-of-arrival methods (doa) and time difference of arrival (tdoa) position location technique," in *Radio Science Conference, 2005. NRSC 2005. Proceedings of the Twenty-Second National*, March 2005, pp. 173–182.

[16] N. Alsindi, B. Alavi, and K. Pahlavan, "Measurement and modeling of ultrawideband toa-based ranging in indoor multipath environments," *Vehicular Technology, IEEE Transactions on*, vol. 58, no. 3, pp. 1046–1058, March 2009.

[17] G. Reddy, "Indoor uwb communication system model," *International Journal Of ENGINEERING SCIENCES AND RESEARCH TECHNOLOGY*, vol. 3, no. 11, pp. 45–50, November 2014.

[18] I. Valera, B. T. Sieskul, and J. Míguez, "On the maximum likelihood estimation of the toa under an imperfect path loss exponent," *EURASIP Journal on Wireless Communications and Networking*, vol. 2013, no. 1, pp. 1–21, 2013.

[19] W. Wang, T. Jost, C. Mensing, and A. Dammann, "Toa and tdoa error models for nlos propagation based on outdoor to indoor channel measurement," in *Wireless Communications and Networking Conference, 2009. WCNC 2009. IEEE*, April 2009, pp. 1–6.

[20] O. Bialer, D. Raphaeli, and A. Weiss, "Efficient time of arrival estimation algorithm achieving maximum likelihood performance in dense multipath," *Signal Processing, IEEE Transactions on*, vol. 60, no. 3, pp. 1241–1252, March 2012.

[21] D. Dardari, C. Chong, and M. Win, "Threshold-based time-of-arrival estimators in uwb dense multipath channels," *Communications, IEEE Transactions on*, vol. 56, no. 8, pp. 1366–1378, August 2008.

[22] W. Liu, H. Ding, X. Huang, and Z. Liu, "Toa estimation in ir uwb ranging with energy detection receiver using received signal characteristics," *Communications Letters, IEEE*, vol. 16, no. 5, pp. 738–741, May 2012.

[23] A. Maali, A. Mesloub, M. Djeddou, H. Mimoun, G. Baudoin, and A. Ouldali, "Adaptive ca-cfar threshold for non-coherent ir-uwb energy detector receivers," *Communications Letters, IEEE*, vol. 13, no. 12, pp. 959–961, December 2009.

[24] G. Mao, B. Fidan, G. Mao, and B. Fidan, *Localization Algorithms and Strategies for Wireless Sensor Networks*. Hershey, PA: Information Science Reference - Imprint of: IGI Publishing, 2009.

[25] T. Davis, *MATLAB primer*. CRC press, 2010.

[26] H. Meikle, *Modern Radar Systems(2nd Edition)*. Artech House, 2008.

[27] B. Mahafza, *Radar Systems Analysis and Design Using MATLAB*, 1st ed. Boca Raton, FL, USA: CRC Press, Inc., 2000.